Raman Hyperspectral Imaging Spectrometer Utilizing Crystalline Colloidal Array Photonic Crystal Diffraction

Kyle T. Hufziger, Sergei V. Bykov, Sanford A. Asher*

University of Pittsburgh, Department of Chemistry, 219 Parkman Avenue, Chevron Science Center, Room 701, Pittsburgh, PA 15260 USA

We fabricated a novel hyperspectral Raman imaging spectrometer that, for the first time, uses a photonic-crystal wavelength-selecting device to select a narrow-wavelength spectral interval. The photonic crystal consists of an array of highly charged, monodisperse polystyrene particles that self-assemble into a face-centered cubic crystal. The photonic crystal Bragg-diffracts a narrow spectral interval that can be tuned by altering the incident angle of collimated Raman scattered light. Our prototype spectrometer diffracts a ~200 cm^{-1} interval of the 488 nm excited visible Raman spectrum of Teflon. This enabled us to select a close-lying triplet of Teflon Raman bands. We imaged the Teflon surface by focusing this narrow region onto a charge-coupled device to create a Raman image of the sample surface that spectrally details the chemical composition.

Index Headings: **Visible Raman spectroscopy; Hyperspectral imaging spectrometer; Polystyrene; Nanosphere; Crystalline colloidal array; Photonic crystal.**

INTRODUCTION

Hyperspectral imaging is a powerful technique because it determines the spatial dependence of the sample's chemical composition.[1–3] The spectrum of each pixel in a hyperspectral image is encoded with the sample's surface chemical composition. This information can be used for characterizing pharmaceutical tablets,[4] determining food quality,[5,6] monitoring the atmosphere,[7] and performing standoff detection of analytes.[8] Hyperspectral images have been measured for reflectance,[9] fluorescence,[10] infrared absorbance,[11] and Raman spectral techniques.[12]

Raman spectroscopy is well suited to identifying chemical species because Raman spectra are molecular fingerprints. Raman spectral bands contain vibrational information that details molecular composition and molecular environment.[13] Raman imaging spectrometers can use either mapping techniques or wide-field imaging. Mapping instruments use a focused laser beam and a precision sample translation stage.[14,15] To create an image, the laser is rastered over the sample surface while collecting Raman-scattered light at each desired position. The collected light at each position is dispersed using a traditional Raman spectrometer. Raman spectrometers typically use double or triple monochromators to remove the intense Rayleigh-scattered light. Although these systems provide excellent spectral-resolving power, they often are large, are heavy, and have poor throughput.[16] The consequence is that long integration times and high laser powers must be used to achieve a sufficient signal-to-noise ratio. The resulting accumulation times for rastered Raman images can be extremely long, depending on the desired spatial resolution and the sample size.

Alternatively, wide-field instruments use a broad laser beam and the scattered light is simultaneously collected from a large surface area.[17] Rather than dispersing the collected light with a diffraction grating, these instruments typically use thin-film bandpass filters,[18] acousto-optic filters,[19] or liquid crystal tunable filters[20] to select a narrow-wavelength Raman spectral region for imaging on a charge-coupled device (CCD) camera. The advantage of this approach is that narrow spectral Raman images are created of the entire sample surface, greatly decreasing the total time required to generate the hyperspectral image.

In previous work, we pioneered the use of crystalline colloidal array (CCA) photonic crystals as spectral dispersion optical devices for use as Rayleigh rejection filters in Raman spectrometers.[21–25] More recently, there have been additional studies on the utility of using photonic crystals to replace traditional diffraction gratings.[26–28] In this study, we use photonic crystals for the first time as the wavelength-selecting element of a wide-field Raman imaging spectrometer to diffract narrow spectral regions of light.

EXPERIMENTAL

Synthesis of Monodisperse Polystyrene Nanoparticles. Polystyrene nanospheres were synthesized using a modification[29] of the previous method of Reese et al.[30] A 500 mL jacketed Kontes reaction vessel was temper-

Received 14 May 2014; accepted 24 June 2014.

* Author to whom correspondence should be sent. E-mail: asher@pitt.edu.

DOI: 10.1366/14-07599

0003-7028/14/6811-1219/0

ature controlled using a Thermo Neslab RTE 740 recirculator (Thermo Scientific) and stirred by using a BDC6015 overhead stirrer (Caframo) connected to a Teflon-coated stir rod.

Styrene (Sigma Aldrich) was passed through a column containing 50 mL of aluminum oxide to remove the butylcatechol inhibitor. The ionic comonomer 3-allyloxy-2-hydroxy-1-propanesulfonic acid (COPS-1), the charged surfactant dihexyl sulfosuccinate (MA-80-1), and ammonium persulfate were acquired (Sigma Aldrich), and used as received. Sodium bicarbonate was acquired (J.T. Baker) and used as received. Nanopure water was generated using a Barnstead purification system (Thermo Scientific).

A typical synthesis for the monodisperse 105 nm diameter polystyrene spheres is as follows. We added 0.348 g sodium bicarbonate and 275 mL nanopure water directly to the reaction vessel, which was fitted with an addition funnel, a Teflon stir rod, a nitrogen-purging inlet, and a reflux condenser. The stirring rate was set to 60 rpm, and the solution was deoxygenated for 30 min with nitrogen gas (N_2). We dissolved 3.433 g MA-80-1 in 5 mL nanopure water and added it to the reactor, allowing 10 min of deoxygenating after the addition. We transferred 115 mL styrene to an addition funnel that had previously been wrapped in aluminum foil to prevent photopolymerization. The styrene was purged with N_2 for 30 min. After purging, the stir speed was increased to 350 rpm and the reactor brought to a temperature of 50 °C. The styrene monomer was then added at a rate of ~0.1 mL/s. We added 6.282 g COPS-1 5 min after the completion of styrene addition and increased the temperature to 70 °C. We dissolved 1.562 g ammonium persulfate in 5 mL nanopure water and injected it to initiate the reaction. After allowing the reaction to proceed for 2 h, we injected an additional 1.043 g COPS-1 into the reactor, followed 5 min later by another 1.015 g ammonium persulfate dissolved in 2 mL nanopure water. We allowed the reaction to proceed for another hour before being cooled to 50 °C while stirring. The particle dispersion was then filtered through previously boiled glass wool.

The mixture was then dialyzed using either 14 000 Da molecular weight cut-off (MWCO) regenerated cellulose tubing (Sigma Aldrich) or 1000 kDa MWCO cellulose ester tubing (Millipore) against nanopure water for two weeks. Following dialysis, the polystyrene colloidal dispersion was stored in contact with cleaned AG-501-X8 (Bio-Rad) mixed-bed ion-exchange resin.[31] The colloidal particle concentration was varied by adding or removing water. Care needs to be taken when increasing the concentration to avoid aggregation. To increase the colloid concentration, the particles were placed in 100 kDa MWCO regenerated cellulose centrifugal filters (Millipore Amicon) and spun at 2000 g to slowly draw water from the sample.

Characterization Techniques. The diffraction of the colloidal array was measured using a Cary 5000 UV-Vis-NIR absorption spectrometer. Zeta potentials were measured using a Malvern Nano ZS90 Zetasizer. Particle sizes were measured using a FEI Morgagni 268, 80 kV transmission electron microscope (TEM) by placing 10 μL of the dilute colloidal dispersion on Formvar-coated copper grids (01814-F, Ted Pella) and evaporating to dryness. We measured 100 spheres via ImageJ (National Institutes of Health [NIH]) to determine the particle monodispersity.

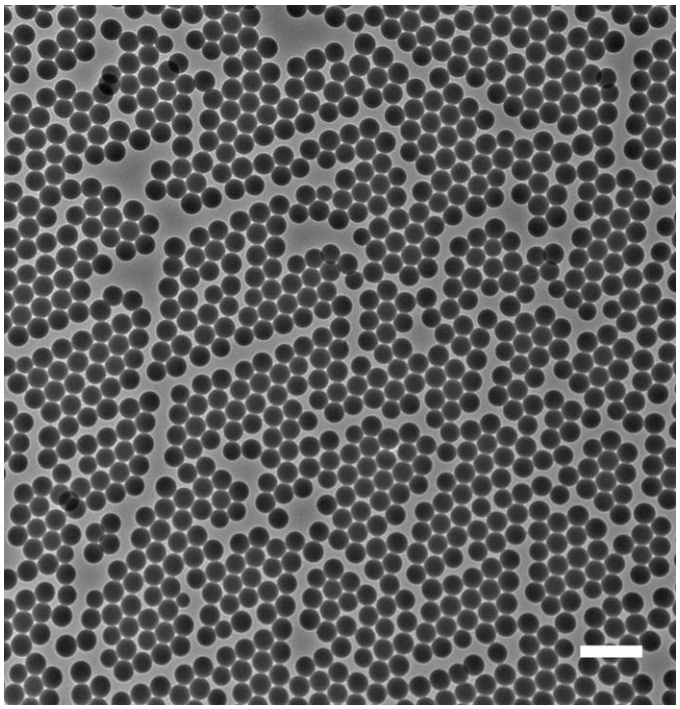

FIG. 1. The TEM micrograph of monodisperse 102.7 ± 4.1 nm diameter polystyrene nanospheres. Scale bar represents 300 nm.

Raman Instrumentation. A Renishaw InVIA Raman microscope using 488 nm excitation was used to measure the Raman spectrum of Teflon. All imaged samples were excited with ~300 mW 488 nm light from a Innova 90C-A6 argon ion laser (Coherent Industries). A HR4000 spectrometer (Ocean Optics) was used to record the diffracted Raman spectra by focusing the light directly into its entrance slit. Raman images were collected using a PyLoN 400 B back-illuminated 1340 × 400 pixel CCD camera (Princeton Instruments), with a pixel size of 20 × 20 μm. The Raman image exposure time was 5 s. Laser power was measured using a TPM-300 power meter (Gentec).

RESULTS AND DISCUSSION

Photonic Crystal Diffraction. We used 102.7 ± 4.1 nm diameter polystyrene spheres that had a zeta potential of −81.8 mV at pH 5 (Fig. 1). This surface charge derives from thousands of negatively charged sulfonate groups from the ionic comonomer COPS-1. These highly charged spheres repel each other and self-assemble in low-ionic-strength solutions into face-centered cubic (FCC) crystals that diffract light according to Bragg's law (Eq. 1).[32]

$$m\lambda_0 = 2nd\sin(\theta) \quad (1)$$

where m is an integer describing the order of diffraction, λ_0 is the wavelength of light in vacuum, n is the refractive index of the system, d is the diffraction plane spacing, and θ is the glancing angle. The value of θ depends on

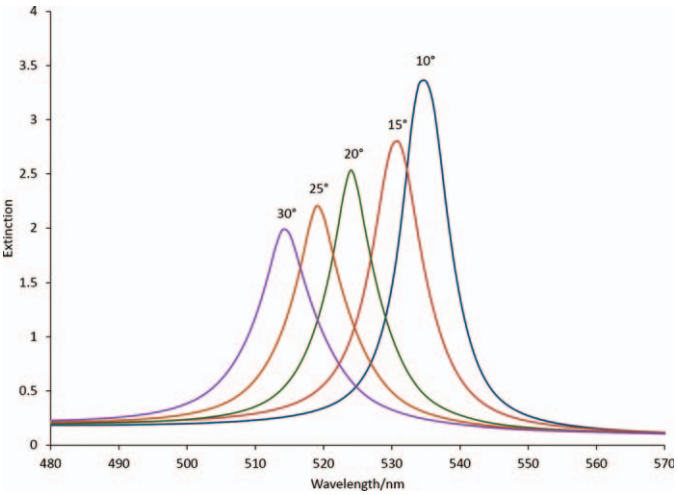

FIG. 2. Incidence angle dependence of diffraction by a 102.7 nm diameter polystyrene particle photonic crystal measured using an absorption spectrometer. Incidence angles measured in air.

any refraction for light entering the photonic crystal. For any plane spacing *d*, only one narrow-wavelength band efficiently diffracts at each incidence angle θ.[33] Other wavelengths not meeting the Bragg condition transmit through the array except for small reflections from the windows enclosing the photonic crystal.

Polystyrene particle self-assembly into photonic crystals occurs readily for particle weight fractions from 2 to 15%. The lattice spacing *d* can be calculated for any desired plane for an FCC crystal of known particle concentration.[34] The diffraction wavelength maximum can be calculated at any incidence angle.[35]

The photonic crystal was contained between two 5.08 cm (2 in) diameter quartz plates separated by a 130 μm thick Parafilm spacer. The input window (Thor Labs BSF2550) was wedge shaped to reflect light out of the diffraction plane. The colloidal particle dispersion was injected into the cavity between the plates, where it immediately assembled into an FCC crystal, resulting in bright iridescence. The photonic crystal used here diffracts a narrow ~9 nm full width half-maximum (FWHM) wavelength band. As the photonic crystal is rotated to achieve different incidence angles, different narrow-wavelength bands diffract (Fig. 2). The band width depends on the CCA ordering and particle diameter. Smaller particles, thinner crystals, and better ordered FCC arrays result in narrower diffraction.[35]

The diffraction efficiency decreases for larger incidence angles due to the decreased diffraction efficiency of π polarized light.[36] In addition, charged impurities can screen the electrostatic repulsive force between particles. This results in disorder that increases the diffraction bandwidth. To maximize diffraction efficiency and minimize band width we used low ionic strength solutions and carefully cleaned quartz cells.

We determined the diffraction efficiency by directing a 514 nm argon laser beam onto the photonic crystal and measuring the diffracted beam intensity using a power meter. Diffuse scattering due to phonon modes and crystal defects are the primary sources of diffraction light loss.[35,37] A 0.5 cm aperture was placed before the

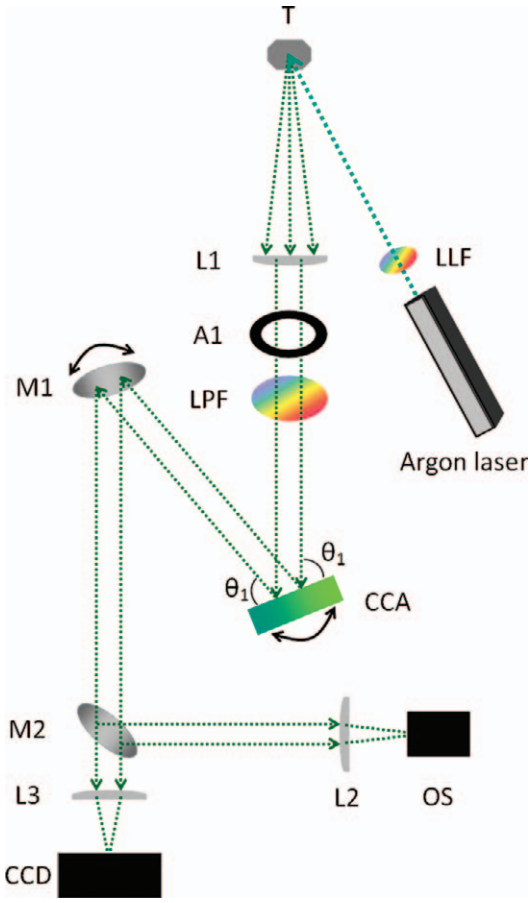

FIG. 3. Diagram of the Raman imaging spectrometer where an argon laser produces 488 nm light. A1, 1.5 cm diameter aperture; CCA, crystalline colloidal array photonic crystal mounted on a rotation stage; CCD, Pylon CCD camera; L1, plano-convex collection lens; LLF, 488 nm laser-line filter; LPF, long-pass edge filter used to remove the Rayleigh-scattered light; M1, rotatable planar mirror; M2, planar mirror used to direct the diffracted light toward either of the plano-convex lenses, L2 or L3; OS, Ocean Optics spectrometer; T, Teflon sample. The lens focal lengths are $f_{L1} = f_{L2} = 10$ cm and $f_{L3} = 30$ cm.

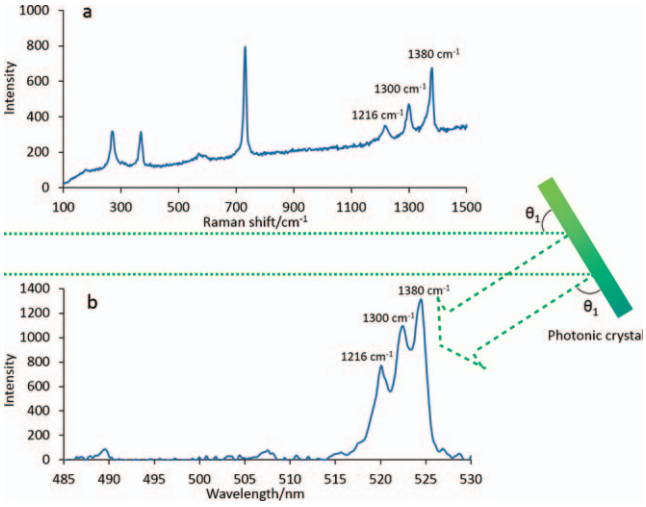

FIG. 4. (**a**) Teflon Raman spectrum measured using the Raman microscope. (**b**) Teflon Raman spectrum of light diffracted by the photonic crystal measured using the Ocean Optics spectrometer. Both samples were excited with 488 nm light.

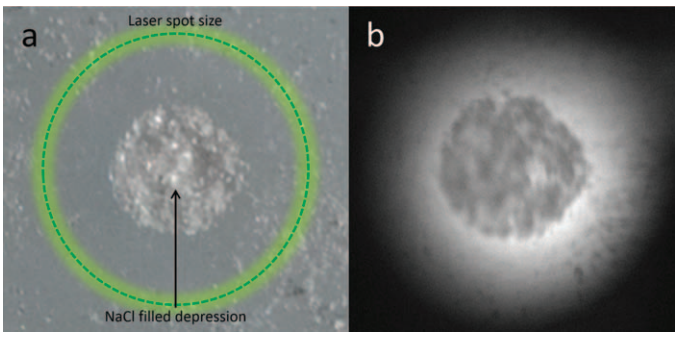

FIG. 5. (**a**) Photograph of a Teflon surface with a ~1 mm diameter NaCl-filled depression. (**b**) Raman spectral image of 1200–1400 cm^{-1} light diffracted by the photonic crystal showing the NaCl-filled depression. Accumulation time for the Raman image was 5 s.

detector to reject some of the diffusely scattered light. We measured an 70% diffraction efficiency for 514 nm light.

Spectrometer Design. The sample was excited using a 488 nm laser beam (Fig. 3) and the backscattered light was collected and collimated using plano-convex lens L1. A thin-film interference long-pass edge filter (Semrock) removed most of the Rayleigh-scattered light. Aperture A1 limited the beam width that illuminated the photonic crystal. The Raman imaging spectrometer used our photonic crystal to select and diffract a narrow-wavelength spectral region. We chose angle θ_1 to select the wavelength of the diffracted spectral region.

Mirror M1 directed the diffracted beam toward mirror M2, which directed it toward either the Ocean Optics spectrometer, to measure the diffracted Raman spectrum, or to lens L3, to focus the collimated narrow wavelength band to form an image on the Pylon CCD camera.

Raman Diffraction. We used a block of polytetrafluoroethylene (Teflon) as a sample. Figure 4a shows the Raman spectrum of Teflon measured using a Raman microscope and 488 nm excitation. Teflon shows strong lines at 731, 1216, 1300, and 1380 cm^{-1} as well as a background probably due to fluorescence. We selected the triplet centered at ~1300 cm^{-1} (522 nm) for imaging and angle-tuned the photonic crystal to diffract a band of light centered at 522 nm.

Figure 4b shows the Raman spectrum of the diffracted light that was focused onto the slit of the Ocean Optics spectrometer. We can clearly see the triplet of Teflon bands centered at 522 nm. Most of the light below 517 nm and above 527 nm was transmitted through the photonic crystal, except for a small amount scattered by the polystyrene spheres and reflected by the quartz cell surfaces.

Raman Imaging. Our Raman imaging measurements used a Teflon sample that contained a ~1 mm diameter circular depression filled with finely ground sodium chloride (NaCl; Sigma Aldrich) (Fig. 5a). Sodium chloride was used because it shows no Raman bands in the ~1300 cm^{-1} spectral region. The sample surface was illuminated using a ~2 mm diameter 488 nm laser beam.

The Raman light diffracted by the photonic crystal was imaged using lens L3 onto the CCD, resulting in a Raman image of the sample surface. Lens L3 magnified the image on the CCD by ~3 to increase image resolution. Due to the Teflon Raman bands centered at ~1300 cm^{-1}, the Teflon surface appears bright, while the NaCl-filled center is dark (Fig. 5b).

Our photonic crystal can be angle-tuned to select and image different narrow-wavelength spectral regions. These images can be accumulated to form a hyperspectral data set that contains a Raman spectrum associated with each pixel. The wavelength range of our spectrometer is limited by the useful spectral range of the photonic crystal, which can be used for incidence angles between 5 and 40°. This enables diffraction measurements over a 1900 cm^{-1} region of the visible spectrum between 490 and 540 nm for the photonic crystal used here. Incidence angles greater than 40° are less useful because they show simultaneous diffraction from higher Miller-index FCC planes.[37]

The diffraction bandwidth calculated using dynamical diffraction theory[38] for 102.7 nm spheres is ~10 nm at 10° incidence, which is in excellent agreement with our measured value (Fig. 2). The photonic-crystal diffraction wavelength bandwidth used here is still relatively broad. It should be significantly narrowed to less than 10 cm^{-1} for maximum-resolution Raman imaging. The diffraction bandwidth can be decreased by decreasing the particle diameter,[37] by increasing particle size monodispersity, by increasing the array ordering, by decreasing the crystal thickness, and by decreasing the difference in refractive index between the particles and the medium. The polystyrene particles used here are suitable for visible and infrared diffracting[39] photonic crystals, but materials such as silica must be used for ultraviolet (UV) light diffraction because polystyrene absorbs below 350 nm.[25]

Work is now ongoing to decrease the diffraction band width of our photonic crystals. We recently demonstrated that 50 nm diameter silica nanosphere photonic crystals diffract ~4 nm FWHM spectral regions in the 230 nm UV spectral region, enabling the construction of a UV Raman photonic crystal imaging spectrometer.[25]

A major advantage of our photonic crystal imaging Raman spectrometer is its relative simplicity and efficiency compared to traditional grating spectrometers. We calculate that, with the use of antireflection-coated lenses and dielectric mirrors, the optimum throughput of our spectrometer would be limited mainly by the diffraction efficiency of the photonic crystal, which we measured to be 70%. Our photonic crystals can also be used as Rayleigh rejection filters in low-cost Raman spectrometers.

CONCLUSION

We demonstrate a prototype Raman imaging spectrometer that uses a photonic crystal consisting of an FCC array of charged polystyrene spheres to diffract a narrow spectral region. Focusing this diffracted Raman light onto a CCD camera generates a Raman image that can be used to determine the surface chemical composition. We are presently working on increasing the spectral resolution and are extending the utility of this approach to the deep UV spectral region.

ACKNOWLEDGMENT

This work was supported by the ONR N00014-12-1-0021 grant.

1. J.M. Amigo. "Practical Issues of Hyperspectral Imaging Analysis of Solid Dosage Forms". Anal. Bioanal. Chem. 2010. 398(1): 93-109.
2. C.-I. Chang. Hyperspectral Imaging: Techniques for Spectral Detection and Classification. New York: Kluwer Academic/Plenum Publishers, 2003. Pp. 1-16.
3. M. Nelson, P. Treado. "Raman Imaging Instrumentation". In: S. Sasic, Y. Ozaki, editors. Raman, Infrared, and Near-Infrared Chemical Imaging New York: John Wiley & Sons, 2011. Pp. 23-51.
4. Y. Roggo, A. Edmond, P. Chalus, M. Ulmschneider. "Infrared Hyperspectral Imaging for Qualitative Analysis of Pharmaceutical Solid Forms". Anal. Chim. Acta. 2005. 535(1-2): 79-87.
5. P.M. Mehl, Y.-R. Chen, M.S. Kim, D.E. Chan. "Development of Hyperspectral Imaging Technique for the Detection of Apple Surface Defects and Contaminations". J. Food Eng. 2004. 61(1): 67-81.
6. H. Huang, L. Liu, M.O. Ngadi, C. Gariépy, S.O. Prasher. "Near-Infrared Spectral Image Analysis of Pork Marbling Based on Gabor Filter and Wide Line Detector Techniques". Appl. Spectrosc. 2014. 68(3): 332-339.
7. R.O. Green, M.L. Eastwood, C.M. Sarture, T.G. Chrien, M. Aronsson, B.J. Chippendale, J.A. Faust, B.E. Pavri, C.J. Chovit, M. Solis, M.R. Olah, O. Williams. "Imaging Spectroscopy and the Airborne Visible/Infrared Imaging Spectrometer (AVIRIS)". Remote Sens. Environ. 1998. 65(3): 227-248.
8. M.T. Bremer, P.J. Wrzesinski, N. Butcher, V.V. Lozovoy, M. Dantus. "Highly Selective Standoff Detection and Imaging of Trace Chemicals in a Complex Background Using Single-Beam Coherent Anti-Stokes Raman Scattering". Appl. Phys. Lett. 2011. 99(10): 1-3.
9. B. Guo, Y. Wang, C. Peng, H. Zhang, G. Luo, H. Le, C. Gmachl, D. Sivco, M. Peabody, A. Cho. "Laser-Based Mid-Infrared Reflectance Imaging of Biological Tissues". Opt. Express. 2004. 12(1): 208-219.
10. F. Pinaud, X. Michalet, L.A. Bentolila, J.M. Tsay, S. Doose, J.J. Li, G. Iyer, S. Weiss. "Advances in Fluorescence Imaging with Quantum Dot Bio-Probes". Biomaterials. 2006. 27(9): 1679-1687.
11. L.H. Kidder, V.F. Kalasinsky, J.L. Luke, I.W. Levin, E.N. Lewis. "Visualization of Silicone Gel in Human Breast Tissue Using New Infrared Imaging Spectroscopy". Nat. Med. 1997. 3(2): 235-237.
12. S. Keren, C. Zavaleta, Z. Cheng, A. de la Zerda, O. Gheysens, S.S. Gambhir. "Noninvasive Molecular Imaging of Small Living Subjects Using Raman Spectroscopy". Proc. Natl. Acad. Sci. U. S. A. 2008. 105(15): 5844-5849.
13. S.A. Oladepo, K. Xiong, Z. Hong, S.A. Asher, J. Handen, I.K. Lednev. "UV Resonance Raman Investigations of Peptide and Protein Structure and Dynamics". Chem. Rev. 2012. 112(5): 2604-2628.
14. G. Steiner. "Infrared and Raman Spectroscopic Imaging". In: R. Salzer, editor. Biomedical Imaging: Principles and Applications. Hoboken, N.J.: John Wiley and Sons, 2010. Pp. 275-303.
15. C. Krafft, T. Knetschke, A. Siegner, R.H.W. Funk, R. Salzer. "Mapping of Single Cells by Near Infrared Raman Microspectroscopy". Vib. Spectrosc. 2003. 32(1): 75-83.
16. P. Flaugh, S. O'Donnell, S.A. Asher. "Development of a New Optical Wavelength Rejection Filter: Demonstration of Its Utility in Raman Spectroscopy". Appl. Spectrosc. 1984. 38(6): 847-850.
17. K.A. Christensen, N.L. Bradley, M.D. Morris, R.V. Morrison. "Raman Imaging Using a Tunable Dual-Stage Liquid Crystal Fabry-Perot Interferometer". Appl. Spectrosc. 1995. 49(8): 1120-1125.
18. M. Iga, N. Kakuryu, T. Tanaami, J. Sajiki, K. Isozaki, T. Itoh. "Development of Thin-Film Tunable Band-Pass Filters Based Hyper-Spectral Imaging System Applied for Both Surface Enhanced Raman Scattering and Plasmon Resonance Rayleigh Scattering". Rev. Sci. Instrum. 2012. 83(10): 103707.
19. H.R. Morris, C.C. Hoyt, P.J. Treado. "Imaging Spectrometers for Fluorescence and Raman Microscopy: Acousto-Optic and Liquid Crystal Tunable Filters". Appl. Spectrosc. 1994. 48(7): 857-866.
20. H.R. Morris, C.C. Hoyt, P. Miller, P.J. Treado. "Liquid Crystal Tunable Filter Raman Chemical Imaging". Appl. Spectrosc. 1996. 50(6): 805-811.
21. S.A. Asher. Crystalline Colloidal Narrow and Radiation Filter. US Patent 4632517 A. Filed 1983. Issued 1986.
22. S.A. Asher, G. Haacke, L.G. Magliocco, H.P. Panzer. Narrow Band Radiation Filter Films. US Patent 5266238 A. Filed 1990. Issued 1993.
23. L. Giovanni, H.P. Panzer. Narrow Band Radiation Filter Films. US Patent 5330685 A. Filed 1991. Issued 1994.
24. S.A. Asher, P. Flaugh. "Crystalline Colloidal Bragg Diffraction Devices: The Basis for a New Generation of Raman Instrumentation". Spectroscopy. 1986. 1(12): 26-31.
25. L. Wang, A. Tikhonov, S.A. Asher. "Silica Crystalline Colloidal Array Deep Ultraviolet Narrow-Band Diffraction Devices". Appl. Spectrosc. 2012. 66(4): 426-431.
26. S.A. Asher, L. Wang, D. Tuschel. Crystalline Colloidal Array Deep UV Narrow Band Radiation Filter. US Patent 20120062883 A1. Filed 2011.
27. S.-H. Kim, H.S. Park, J.H. Choi, J.W. Shim, S.-M. Yang. "Integration of Colloidal Photonic Crystals Toward Miniaturized Spectrometers". Adv. Mater. 2010. 22(9): 946-950.
28. H. Ding, C. Liu, H. Gu, Y. Zhao, B. Wang, Z. Gu. "Responsive Colloidal Crystal for Spectrometer Grating". ACS Photonics. 2014. 1(2): 121-126.
29. M.M. Ward Muscatello, L.E. Stunja, S.A. Asher. "Polymerized Crystalline Colloidal Array Sensing of High Glucose Concentrations". Anal. Chem. 2009. 81(12): 4978-4986.
30. C. Reese, C. Guerrero, J. Weissman, K. Lee, S. Asher. "Synthesis of Highly Charged, Monodisperse Polystyrene Colloidal Particles for the Fabrication of Photonic Crystals". J. Colloid Interf. Sci. 2000. 232(1): 76-80.
31. H.J. Van Den Hul, J.W. Vanderhoff. "The Characterization of Latex Particle Surfaces by Ion Exchange and Conductometric Titration". J. Electroanal. Chem. Interfacial Electrochem. 1972. 37(1): 161-182.
32. L. Liu, P. Li, S.A. Asher. "Fortuitously Superimposed Lattice Plane Secondary Diffraction from Crystalline Colloidal Arrays". J. Am. Chem. Soc. 1997. 119(11): 2729-2732.
33. C. Kittel. Introduction to Solid State Physics. New York: John Wiley, 1971. 4th ed., pp. 1-76.
34. R.J. Carlson, S.A. Asher. "Characterization of Optical Diffraction and Crystal Structure in Monodisperse Polystyrene Colloids". Appl. Spectrosc. 1984. 38(3): 297-304.
35. P.A. Rundquist, P. Photinos, S. Jagannathan, S.A. Asher. "Dynamical Bragg Diffraction from Crystalline Colloidal Arrays". J. Chem. Phys. 1989. 91(8): 4932-4941.
36. G. Pan, A.K. Sood, S.A. Asher. "Polarization Dependence of Crystalline Colloidal Array Diffraction". J. Appl. Phys. 1998. 84(1): 83-86.
37. S.A. Asher, J.M. Weissman, A. Tikhonov, R.D. Coalson, R. Kesavamoorthy. "Diffraction in Crystalline Colloidal-Array Photonic Crystals". Phys. Rev. E. 2004. 69(6): 066619.
38. R.J. Spry, D.J. Kosan. "Theoretical Analysis of the Crystalline Colloidal Array Filter". Appl. Spectrosc. 1986. 40(6): 782-784.
39. C.E. Reese, S.A. Asher. "Emulsifier-Free Emulsion Polymerization Produces Highly Charged, Monodisperse Particles for Near Infrared Photonic Crystals". J. Colloid Interf. Sci. 2002. 248(1): 41-46.